Interface and temperature dependent magnetic properties in permalloy thin films and tunnel junction structures

J.F.Sierra[1*], V.V.Pryadun[1], S.E.Russek[2], M.García-Hernández[3], F.Mompean[3], R.Rozada[3], O.Chubykalo-Fesenko[3], E.Snoeck[4], G.X.Miao[5], J.S.Moodera[5] F.G.Aliev[1]

[1]Departamento Física de la Materia Condensada and Instituto "Nicolás Cabrera"Ciencia de Materiales, Universidad Autónoma de Madrid, 28049 Madrid, Spain.

[2]National Institute of Standards and Technology, Boulder, Colorado 80305, USA.

[3]Instituto de Ciencia de Materiales Madrid, CSIC, Cantoblanco, 28049 Madrid, Spain.

[4]Groupe NanoMatériaux CEMES-CNRS, 29 Rue Jeanne Marvig, Toulouse 31045, France**.**

[5]Francis Bitter Magnet Laboratory, Massachusetts Institute of Technology, Cambridge, Massachusetts 02139, USA.

Date of Submission: 26 October 2010; **Date of Acceptance**: 8 March 2011; **email address**: juanfrancisco.sierra@gmail.com

Abstract

Magnetization dynamics and field dependent magnetization of different devices based on 25-30 nm thick Permalloy (Py) films: such as single Py layers (Py/MgO; Py/CoFeB/Al_2O_3) and Py inserted as a magnetic layer in magnetic tunnel junctions (Py/CoFe/Al_2O_3/CoFe; Py/CoFeB/Al_2O_3/CoFe; Py/MgO/Fe) have been extensively studied within a temperature range between 300K down to 5K. The dynamic response was investigated in the linear regime measuring the ferromagnetic resonance response of the Py layers using broadband vector network analyzer technique. Both the static and the dynamic properties suggest the possible presence of a thermally induced spin reorientation transition in the Py interface at temperatures around 60K in the all samples investigated. It seems, however, that the details of the interface between Py and the hardening ferromagnet/insulator structure, the atomic structure of Py layers (amorphous vs. textured) as well as the presence of dipolar coupling through the insulating barrier in the magnetic tunnel junction structures could strongly influence this low temperature reorientation transition. Our conclusions are indirectly supported by structural characterization of the samples by means of X-Ray diffraction and high resolution transmission electron microscopy techniques. Micromagnetic simulations indicate the possibility of strongly enhanced surface anisotropy in thin Py films CoFe or CoFeB underlayers. Comparison of the simulations with experimental results also show that the thermally-induced spin reorientation transition could be characterized by the presence of strong disorder at the surface.

* Present address. CEA/SPINTEC, 17 Rue des Martyrs, 38054 Grenoble, France, juan.sierra@cea.fr

1. INTRODUCTION

In the last decade advances in nanoscience and nanotechnology have permitted growth of ultrathin ferromagnetic layers. This achievement is nowadays widely used to fabricate new generations of magnetic devices based on magnetic multilayer structures, magnetic nanopillars, or magnetic nanodots, and magnetic patterned media.[1-4] This miniaturization may produce changes not only in the transport properties but also in the magnetization configuration and in the magnetization dynamics of the ferromagnetic layers inside magnetic tunnel junctions (MTJs) in comparison with their bulk properties. It has been previously established that in thin magnetic films the spontaneous magnetization direction is governed by the competition of different contributions to the free-energy functional of the system, namely: intrinsic magneto-crystalline anisotropy, shape anisotropy and surface anisotropy energies.[5] It may be expected that the competition between these energies would be also of significant importance when thin magnetic films are inserted in multilayer structures. Indeed, perpendicular magnetization in ultrathin (few Å) Co layers has been reported for Co/Pd and Co/Pt multilayers,[6] these are implemented in new generation of spintronic devices as spin torque nano-oscillators.[7]

The ground state of the magnetization in magnetic films with intermediate (tens of nm) thickness may be, qualitatively different from those found in bulk materials and ultrathin films. In bulk materials the magnetization direction is determined by microscopic features such as the exchange interaction and the spin-orbit coupling, being both the source of the magnetic anisotropies. In ultrathin films the mechanisms that control the magnetization direction are the shape (demagnetizing fields) and the surface anisotropies, rendering either in-plane or out-of-plane magnetization configurations. Although, in general, thin films present an in-plane magnetization due to the shape anisotropy, for some specific conditions the shape anisotropy could be overcome by surface anisotropies making the magnetization vector to lay out of the thin film plane. The dependence of these energies with film thickness, pressure, temperature or strain alter the competition between shape and surface anisotropies which, in turn, triggers a spin reorientation transition (SRT) from in-plane to out-of-plane or viceversa.[5,8] Focusing on the thermally induced SRT (T-SRT) one observes that while at room temperature the shape anisotropy is the term that determines the magnetization direction, at low temperature is the surface anisotropy.[9] Such T-SRT has been intensively studied for *ultrathin films* including Fe/Cu,[10] Ni/Cu,[11] Gd/W[12] structures and Co/Pd multilayers.[13] Little is known about the T-SRT in thicker (tens of monolayers) single magnetic films grown either on single crystal epitaxial and amorphous layers or when incorporated into spintronic devices, specifically in MTJs. In the latter case the dipolar coupling between the top and the bottom magnetic electrodes could induce novel unexpected phenomena.

Due to its high magnetic susceptibility, low coercive field and small magnetic anisotropy Permalloy (Py: $Ni_{80}Fe_{20}$) is one of the most commonly used magnetic materials in ultra-low magnetic field sensor technologies. Magnetization dynamics of single-layer and exchanged biased Py films (Py/IrMn, Py/CoO and Py/NiO) have been

intensively studied in the last years using ferromagnetic resonance (FMR) experiments at room temperature[14-18] through a wide range of temperatures.[19-21] It was found that in single-layer Py films the dependence with temperature of the resonance frequency and the corresponding linewidth shows an anomalous increase below a critical temperature of 100K.[19,20] This unexpected behavior was interpreted within the framework of the valence exchange and exchange anisotropy mechanisms[19] or, alternatively, due to a T-SRT.[20] In the framework of T-SRT the main effect of temperature on the magnetic properties of Py films was to increase the in-plane uniaxial anisotropy and to induce a surface anisotropy that pushes the magnetization out-of-plane in the Py interface. Recently, in MTJs based on Py free layers, the strong influence of the dynamic properties on the T-SRT has been evidenced.[22] However, with the exception of refs. 20 and 22, little is known about a possible T-SRT in structures based on Py layers.

In order to address the possible effects of different interfaces on the T-SRT in Py *we present an extensive and systematic study of both the magnetization dynamics (using the FMR technique) and the static properties (M vs. H) in different Py-based magnetic structures*: (i) single-layer Py thin films deposited on epitaxial MgO and on amorphous FeCoB/Al_2O_3 substrates and, (ii) Py layers inserted into MTJs with epitaxial MgO or amorphous Al_2O_3 tunnel barriers. Comparatively to the previous work,[22] our new studies include single layers films and MTJs where Py is grown on epitaxial substrates, *i.e* highly ordered Py interfaces, thus showing unambiguously the decisive role of the surface anisotropy. Independently of the substrate morphology, all single-layer Py films show a gradual increase of the resonance frequency with decreasing temperature as well as a clear anomaly in the magnetization curves close to a critical temperature T_R of 60K. Static and dynamics properties of MTJs at low temperatures show, however, more exotic behavior. While dynamic properties of Py grown on epitaxial MgO barrier also exhibit a gradual increase of the resonance frequency with decreasing temperatures a peak in the static properties qualitatively similar to those observed in single-layer Py films but shifted to higher temperatures is observed. MTJs with amorphous Al_2O_3 barriers present a sharp increase in the resonance frequency with a "knee-like" enhancement and a strong anomaly in the static properties at 60K. These results are explained in the framework of a thermally induced spin reorientation transition in the Py interface and the effects of the dipolar coupling between Py and the second magnetic layer in the MTJs. The magnetic moments in the Py interface changes from an in-plane configuration at room temperature to an out-of-plane configuration at low temperatures. Such reorientation goes through a "ripple-like" structure on the surface close to the reorientation temperature T_R due to the competition of different magnetic anisotropies and/or the dipolar coupling in tunnel junction structures. Our model is supported by correlation between the magnitude of the changes both in FMR and magnetization at low temperatures and the degree of crystallinity of the Py layers. This scenario is also supported by X-Ray diffraction experiments and high resolution transmission electron microscopy images. Finally, we perform micromagnetic simulations of hysteresis processes in Py films with surface anisotropy and discuss the obtained results in relation to the experimental observations.

2. EXPERIMENTAL DETAILS

FMR measurements through a wide temperature range (2K<T<300K) were carried out using vector network analyzer (VNA) technique. This technique is based on the excitation of the uniform resonance mode, characterized by its frequency f_0 and its linewidth Δf_0 (defined as the full width at half maximum of the uniform resonance peak) Recent reported works have shown the convenience of this method to investigate the quality of complex layered systems as magnetic multilayer structures.[23]

An AGILENT-E5071B vector network analyzer with a frequency range from 300 kHz up to 8.5 GHz was used in our experiments. In order to create the pumping field h_{rf} that excites the magnetization we use a grounded coplanar wave guide transmission line. The cryogenic environment was created with a Janis variable temperature cryostat and a special designed rf-insert. The sample was mounted on top of the wave guide, and placed inside of a superconducting electromagnet that creates a magnetic field along the easy-axis of the sample. In order to observe the FMR condition the h_{rf} was applied transverse to the applied magnetic field, with both fields in the sample surface. The resonance condition was extracted following the method developed in ref. 18 by means of the scattering matrix parameters provided by the VNA.

The magnetization curves were measured at fixes temperatures between -0.5T and 0.5T in steps of 0.5mT by using a QUANTUM DESIGN superconducting quantum interference device magnetometer (SQUID). The morphology and the quality of the structures were investigated analyzing the X-Ray diffraction patterns while transmission electron microscopy (TEM) images were obtained in a FEI-F20 microscope fitted with a spherical aberration (Cs) corrector (CEOS) whose point resolution is 0.12 nm. Further experimental details will be explained in the corresponding paragraphs below.

3. SAMPLE GROWTH AND CHARACTERIZATION

We shall divide the samples investigated in two sub-classes depending on the type (amorphous vs. single crystal or epitaxial) of the substrates/underlayers on which the magnetically free layer of Py is deposited.

3.1. Py films on amorphous substrates/underlayers

Amorphous MTJs (A-MTJ1 and A-MTJ2) and amorphous single-layer film (further A-SL) were grown on quartz wafers in a high vacuum sputtering chamber with a base pressure of 10^{-9} Torr. Room temperature layers deposition was held in an 18mT magnetic field along the surface layers. After that, an in-situ 250 °C annealing for one hour in the presence of an in-plane magnetic field of 20 mT was done. The structures of both amorphous tunnel junctions are as follows (thickness in nanometers):

A-MTJ1: Ta(5)/Cu(5)/Ta(5)/Ru(2)/$Ir_{20}Mn_{80}$(10)/$Co_{90}Fe_{10}$(3)/Al_2O_3(1.8)/$Co_{90}Fe_{10}$(3)/$Ni_{80}Fe_{20}$(28)/Ta(5)/Ru(5).

A-MTJ2: Ta(5)/Cu(5)/Ta(5)/Ru(2)/$Ir_{20}Mn_{80}$(10)/$Co_{90}Fe_{10}$(3)/Al_2O_3(1.8)/$Co_{60}Fe_{20}B_{20}$(2)/$Ni_{80}Fe_{20}$(23)/Ta(5)/Ru(5).

Both A-MTJs have a CoFe(3) pinned layer that is exchange biased by a naturally IrMn(10) antiferromagnetic layer. The layer composition and thickness of the free layer in both magnetic tunnel junctions were optimized for low magnetic field sensor applications (further details in the sample preparation can be seen in Ref.24).

The A-SL was grown in the same sputtering chamber using the same growth parameters. The single-layer film consists of an Al_2O_3(1.8)/ $Co_{60}Fe_{20}B_{20}$(2)/$Ni_{80}Fe_{20}$ (23)/Ta(5)/Ru(5) stack, similar to the free layer of A-MTJ2.

3.2. Py films grown on epitaxial MgO buffer layers

The fabrication of epitaxial structures was done in a molecular beam epitaxy system with a base pressure of 10^{-10} torr. The epitaxial MTJ (further E-MTJ) stack has the following composition: MgO(10)/Fe(20)/MgO(5)/$Ni_{80}Fe_{20}$(30)/Al_2O_3(5), while the epitaxial single-layer (further E-SL) has the following structure: MgO(10)/$Ni_{80}Fe_{20}$(30)/Al_2O_3(5). Both samples were covered with 5nm thin Al_2O_3 capping layer. In order guarantee the epitaxial grown of MgO on Si substrates, firstly a 10nm MgO buffer layer at 300°C at ~0.06 Å/s was deposited. Then it was cooled down to 180°C, and, in the case of E-MTJ the 20 nm Fe layer was deposited at ~0.08 Å/s. The 5 nm MgO barrier was deposited at 180°C at 0.06 Å /s. Afterwards, the sample was heated to 280°C and the Py was deposited at 0.1 Å/s. The Al_2O_3 capping layer was deposited at room temperature (see Ref. 25 for sample growth details).

3.3. TEM images

Figure 1(a)-(b) shows the cross-section images using low magnification and high resolution TEM technique for two of the amorphous structures studied (A-MTJ2 and A-SL).

The examination of the TEM images in the Al_2O_3/$Co_{60}Fe_{20}B_{20}$/Py single-layer indicates that Py is (111) textured while the CoFeB/Al_2O_3 bilayer is amorphous.

On the one hand, TEM analysis in the amorphous tunnel junction 1 (A-MTJ1) shows an $Ir_{20}Mn_{80}$/$Co_{90}Fe_{10}$ pinned layer (111) textured. The Al_2O_3 insulating barrier is amorphous and very rough. Finally, in the $Co_{90}Fe_{10}$/Py layer it is difficult to observe a texture in the CoFe while the upper Py layer is (111) weakly textured. On the other hand, in the amorphous tunnel junction 2 (A-MTJ2) the $Ir_{20}Mn_{80}$/$Co_{90}Fe_{10}$ pinned layer has less imperfections than in A-MTJ1 with a highly (111) texture. The Al_2O_3 insulating barrier is amorphous with smaller roughness. In the $Co_{90}Fe_{10}B_{20}$/Py free layer we observe that $Co_{60}Fe_{20}B_{20}$ seems to be amorphous and the upper Py layer highly (111) textured.

We note that both amorphous tunnel junctions present an *anticorrelated roughness* (see regions marked with arrows in Fig. 1(b)). The presence of this anticorrelated roughness has a strong influence in the T-SRT mechanism as will be discussed later.

The TEM images of epitaxial structures -E-SL and E-MTJ- are shown in Fig. 2(a)-(b) respectively. Both structures present an epitaxial (001) MgO deposition on Si wafers and polycrystalline structure of the Py layer. The E-MTJ exhibits an epitaxial growth of both Fe and MgO barrier layers (both in the crystallographic (001) direction). We shall discuss below, however, the possibility of some weak texture of this E-SL at its interface with epitaxial MgO (001) to explain the experimental findings.

3.4. X-Ray diffraction experiments

In order to have more detailed information on the layer morphology of the samples X-Ray diffraction (XRD) experiments were carried out.

XRD measurements on amorphous samples were investigated using Cu Kα radiation on a BRUKER-D8 θ-θ diffractometer equipped with a position sensitive detector and a Ni filter to suppress Cu Kβ radiation. Samples were mounted on glass sample-holders and those grown on Si were slightly misaligned to prevent strong reflections from the single crystal substrates reaching the detector while θ-2θ scans were performed. Figure 3 summarises the results obtained for amorphous samples. For A-MTJ1, four diffraction peaks between 2θ =40 and 45 degrees are prominent. Based on a structural database search we have assigned these peaks as arising from IrMn(111), Ru (002), Cu(111) and Py (111). However, only two of them (IrMn (111) and Py(111)), are clearly present in A-MTJ2. In the case of the A-SL film, we have identified again the peak from the Py (111) planes from a f.c.c. structure at 2θ=44.4 degrees. We note the absence of other diffraction peaks from the Py layer concluding the preferential (111) orientation of the Py in the amorphous samples.

XRD for epitaxial structures was done in a RIGAKU-RU300 diffractometer using a Cu $K\alpha$ radiation. From Fig.4 one clearly observes the peak from Py (111) planes as well as peaks coming from (200) and Py (220) planes, which appear near 2θ =51 and 75 degrees respectively indicating its polycrystalline structure.

4. EXPERIMENTAL RESULTS

4.1. Dynamic properties

We have evaluated the real and the imaginary parts of the complex parameter U(f), which are proportional to the dispersion and the loss profiles of the FMR spectrum respectively.[18] The FMR spectrum is characterized by its resonance frequency f_0 and its linewidth Δf_0 whose experimental values can be extracted from the Im[U(f)]. We note that in the case of MTs the measured values of f_0 and Δf_0 correspond to the excitation of the free layer magnetizations: CoFe/Py and

CoFeB/Py for A-MTJ1and A-MTJ2 respectively and Py for E-MTJ. The detection of the FMR peak in the pinned layer requires higher fields that have not been used here.

Figures 5(a)-(b) show the value of Im[U(f)] for the amorphous tunnel junctions, AMTJ-1 and AMTJ-2, respectively. Here we show he representative spectra at low (5K) and room temperature measured in an applied field of $\mu_0 H_{ap}$ =20mT. On the one hand, at room temperature the FMR frequency follows the Kittel equation $f_0=(\gamma\mu_0/2\pi)[(H_K+M_S+H_{ap})(H_K+H_{ap})]^{1/2}$, where γ is the gyromagnetic ratio ($1.76\cdot10^{11}$ s^{-1} T^{-1}), H_K is the anisotropy field and M_S the saturation magnetization (see Figs. 5(c)-(d)). On the other hand, f_0 shifts to higher values when the sample was cooled in zero magnetic field (ZFC). From the Kittel equation we extracted the values of $\mu_0 M_S$ and $\mu_0 H_K$ at room temperature. While for both tunnel junctions the value of $\mu_0 M_S$=1.17 T the anisotropy field changes from $\mu_0 H_K$=1.75 mT for A-MTJ1 to $\mu_0 H_K$=1.52 mT for A-MTJ2. The bulk of the free layer anisotropy arises from the coupling of the pinned layer and the free layer and reduction in the anisotropy field indicates a reduction in this coupling. At low temperatures f_0 follows a Kittel-like behavior. However, the extraction of M_S and H_K from the Kittel equation is not possible since the magnetization was not fully saturated in-plane.

These two facts are summarized in Figs. 6(a)-(b), where the contour plots of the resonance frequency as a function of temperature and magnetic field in the 0mT $\leq\mu_0 H_{ap}\leq$60mT field range is plotted.

We plot f_0 vs. T for the amorphous tunnel junctions at different applied fields in figs. 6(c)-(d). Although the temperature dependences f_0 (T) is less pronounced for A-MTJ2 both samples reveal a well defined "knee-like" enhancement below roughly T_R~60K.

Figures 7(a)-(b) show the contour plots of the free-layer FMR linewidth (Δf_0) as a function of temperature and applied field for amorphous magnetic tunnel junction A-MTJ1 and A-MTJ2 respectively. As illustrates Figs. 7(c)-(d), Δf_0 vs. T reveal an abrupt variation close to T_R. The A-MTJ1 linewidth gradually increases with decreasing temperature down to T_R. At this point Δf_0 suddenly increases reaching a maximum value at 25K and then suddenly decreases at a value similar to those measured at room temperature. On the other hand for the A-MTJ2 the increasing linewidth with decreasing temperature is observed down to T_R, then an abrupt decreasing in the linewidth is clearly observed below T_R.

We should point out that the measured anomalous temperature dependences in the FMR properties of Py layers in MTJs were found to be practically independent of the field history. Since the same temperature dependences were obtained with different field cooling conditions which included a 3T field cooling from 200K to 4K (not shown) and ZFC (actual data). Therefore, we exclude any essential influence of oxide formation in the ferromagnetic layer to these temperatures dependences.

In order to compare the results with A-SL sample we shall consider the A-MTJ2 whose free layer structure is similar to the A-SL. Figures 8(a) and 8(c) respectively show the f_0(T) and the Δf_0 (T) temperatures dependences-measured at $\mu_0 H_{ap}$=20mT. The temperature dependence of f_0 reveals a gradual increase with decreasing temperature in both samples, however, a clear "knee-like" enhancement at T_R~60K is observed in the tunnel junction only. Δf_0 vs. T does not reveal any sharp anomalies in the temperature dependence for A-SL. The fact that the Py free layer structure shows

different temperature dependences of the FMR response when inserted in the multilayer structure evidences the strong influence of the interaction between the free and the pinned layer on the magnetization dynamics of the free layer.

Comparison between temperature dependent dynamic response of Py layers in the epitaxial structures (E-SL and E-MTJ) reveals again a gradual increase of the FMR frequency with decreasing temperature and small changes in Δf_0 with temperature, with values of about 0.2 GHz and 0.28 GHz for E-SL and E-MTJ respectively (see Fig. 8(d)).

4.2 Static properties

The magnetization curves were measured cooling the samples in zero applied field to the lowest temperature (5K), followed by an application of the magnetic field after each new temperature stabilization has been reached. The magnetization hysteresis loops were measured from 0.5T to -0.5T (decreasing field branch) and from -0.5T to 0.5T (increasing field branch) and each cycle has been completed at zero field.

Figure 9 illustrates the magnetization vs. magnetic field (M vs. H) for A-MTJ2 and A-SL close to the temperature where the "knee-like" enhancement in f_0 is observed. An unexpected deviation of the magnetization from saturation values close to high field regions of 0.5T is apparent. In the following, we introduce M^*_S=M(0,5T) value measured with the increasing field to describe quantitatively this anomalous behavior. In addition, we have observed that the hysteresis loop corresponding to the fixed layer reversal sharpens above 60K (see differences in the minor hysteresis loops close near -125mT). This effect is an indication of a possible reconfiguration of the magnetic moments in the exchanged biased pinned layer. In the case of the A-SL sample we observe an anomalous variation on M^*_S but quantitative and qualitative different from the observed in the multilayer structure.

These differences are summarized in Fig. 10(a) for tunnel junction structures and Fig. 10(b) for single-layer films. Here the value of M^*_S is normalized by its value at low temperature (5K) and is plotted as a function of the temperature close to the reorientation transition temperature.

We observe that both amorphous MTJs show a peak and a dip anomalies in temperature dependence of M^*_S close to T_R=60K. However, in the case of A-SL, E-SL and E-MTJ samples we observe notably smaller and qualitatively different anomalies in M^*_S (T) with a single peak close to T_R.

The temperature dependence of the coercive field for A-MTJ1 and A-SL, where the normalized M_S vs. temperature exhibits the more pronounced anomalies (peak and dip for A-MTJ1 and maximum for A-SL). As Fig. 11 shows, A-MTJ1 presents a strong increase in H_C with decreasing temperature. This effect may be induced by a non-uniform single-domain particle size distribution in the free layer of A-MTJ1.[26] Interestingly, we also observe a weak anomaly near the reorientation transition. This is mainly evident in the derivative curve (see arrow in the inset of the figure). Alternatively, A-SL presents a constant value of H_C for the temperatures studied.

5. MICROMAGNETIC MODELING OF THE REORIENTATION TRANSITION IN PERMALLOY FILMS.

In this section we present results of the micromagnetic modeling of Py films with surface anisotropy. Our goal is to demonstrate the most important consequences of the temperature-induced spin reorientation transition for static measurements.

The spin reorientation transition is often discussed in the framework of a simplified model, assuming one magnetic moment approximation (see e.g. Refs. 27,28). If θ denotes the angle between the magnetization direction and z-axis, the following expression describes the magnetic energetic balance in a thin film:

$$E = K_s Sa \sin^2\theta - KV \sin^2\theta - \frac{1}{2}\mu_0 M_S^2 \sin^2\theta = K_{eff} V \sin^2\theta \qquad (1)$$

Here K_s is the surface anisotropy value acting on the surface layer with thickness a, S is the magnetic film surface, V its volume and M_s is the saturation magnetization. The last term describes the shape anisotropy of the magnetostatic origin. The appearance of the surface anisotropy is typical for multilayer structures. It results from the presence of the lattice mismatch, internal stresses, the change of electronic structure, the broken bonds and local spin disorder. All these effects are difficult to describe and they are normally embedded in a phenomenological concept of the effective surface anisotropy.

The model is based on the assumption of the homogeneous magnetization in thin film under competing interactions and, therefore, should be valid for ultra-thin films only (film thickness below 4 nm for Py). Clearly, in this approach the thin film magnetization can be described using the effective anisotropy K_{eff} idea. The spin reorientation transition occurs for K_{eff} =0. Naively, it could be thought that near the reorientation transition the bulk magnetocrystalline, the shape and the surface anisotropies compensate each other and the coercive field vanishes. The detailed analysis, however, shows that this is not true.

Indeed, detailed numerical modeling have shown that even in ultra-thin films near the reorientation transition the magnetization pattern can be very complex, consisting, for example, in perpendicularly magnetized stripes[29-31]. The perpendicular magnetized stripes lead to almost zero magnetization near the transition point, the net magnetization then can be considered as decoupled from the Zeeman field and, therefore, the maximum of the coercivity could be expected. As we see, below, this is indeed true in our simulations performed for thin films with thickness above exchange correlation length 4nm.

Our modeling is based on a standard 3D micromagnetic approach with cubic discretization, implemented in our proper code Microm where the magnetostatic energy calculation is performed via the DADI approach.[32,33] Namely, the Py thin film was modeled as a slab of 600 x 600 x 25 nm with periodic in-plane boundary conditions to get a correct thin film demagnetizing field. The energy was minimized by the integration of the Landau-Lifshitz-Gilbert equation of

motion. The following parameters, obtained from the experimental data, were used for the bulk Py: the low-temperature saturation magnetization $\mu_0 M_S$=1.17T, anisotropy field H_K =1.75 mT (anisotropy axis parallel to X), the exchange parameter A=10^{-11} J/m, the Curie temperature T_C=869 K. The surface anisotropy was introduced via an additional layer of 3 nm where the anisotropy on the surface was introduced either perpendicular to the Py thin film or with randomly distributed easy axes. We estimated the surface Curie temperature from the loss of nearest neighbors on the surface (T_C^s=507 K**).** The zero-temperature surface anisotropy value K_s and its Curie temperature T_C^s were taken as adjustable parameters. The magnetization dependence on temperature was evaluated via the Langevin function and the anisotropy – via the common relation from the Callen-Callen theory[34] $K(T) \propto M^3(T)$, the temperature dependence of the surface anisotropy is not known. However, for the case when the surface anisotropy is much stronger than the bulk anisotropy (as in Py case) it has been show to scale with the surface magnetization following the same Callen-Callen law[35] $K_s(T) \propto M_s^3(T)$. This is the assumption that we adopt in the present simulation.

In Fig. 12 we present the results of the coercive field value as a function of temperature in two models. In model A the surface anisotropy value was taken from a coherent rotation model (see Eq. 1). Requiring the temperature-induced magnetization reorientation (from out-of-plane to in-plane) to occur in Eq. (1) at T_R=60 K**,** this approach gives the surface anisotropy value $K_s(T=0)$=1.3 x 10^6 J/m^3**.** Thus, in model A we assume this value of the surface anisotropy and perform 3D micromagnetic simulations. The simulations indicate that the coherent rotation approximation is not valid, since the thickness of the Py thin film is sufficient to fit the domain wall. In fact, the surface layer acts as a pinning layer with perpendicular anisotropy, producing an "exchange-spring" effect (see Fig.13 (a)), responsible for the fact that the coercive field is very slowly dependent on temperature in low temperature range. The reorientation transition occurs at much higher temperature T_R=450 K, at which a strong increase of the coercive field is observed. This increase is associated with the competition between different magnetic contributions (surface magnetic anisotropy against in-plane magnetocrystalline and shape anisotropies), leading to a creation of the "ripple-like" structure on the surface (see Fig. 13 (b)). This structure is the reminiscence of the perpendicular domain structure reported for ultra-thin films[29-31]. The presence of these structures explains the necessity of a larger saturating field for temperatures close to the reorientation transitions, at higher temperatures all spin moments lay in plane.

Although qualitatively model A gives us an insight into the spin-reorientation micromagnetic behavior, the spin reorientation temperature is very high. Model B is the result of the fitting procedure of the micromagnetic model aiming to produce the surface anisotropy parameter resulting in the reorientation transition at T_R= 60K. Thus, we vary the surface anisotropy value until the results match the experimentally observed reorientation temperature. The corresponding value was found to be $K_s(T=0)$=3.4 x 10^5 J/m^3 **(**approximately 1000 times larger than that of the Py). The increase of the coercive field in this model is much more pronounced than that in model A. The magnetic moment

configurations below T_R are the same as presented in Fig.13 (a) and at T_R – as in Fig. 13 (b). Additionally, when we included random easy axes distribution on the surface, this gave a possibility to tune the absolute value of the maximum coercive field.

Our results indicate that the spin reorientation transition is associated with a maximum of the coercive field. This happens due to the fact that exactly at this moment the overall anisotropy (including of the magnetostatic origin) is zero. When comparing the results with the experimental ones, it should be noted that in reality Py has a polycrystalline structure in most samples, where the distribution of local properties may smear out the observed behavior. However, the trace of the maximum of the coercive field is seen in Fig. 11 in A-MTJ1 sample. The real maximum is probably hidden by the sharp increase of the coercive field due to the strong dipolar coupling (via orange peel coupling) between the free and the pinned layer. However, the anomaly clearly seen in the derivative occurs at the same place and with the same magnitude as seen in model B. For the A-SL sample, as well as for E-SL and E-MTJ, which are not shown here, the measured coercive field are almost independent of temperature. This is in accordance with the modeling result and may be interpreted as a reorientation transition above room temperature.

6. DISCUSSION

We start the discussion with a brief resume of previous findings. Initial investigations of the temperature dependent dynamic properties in polycrystalline Py films grown on SiO_2 substrates with film thicknesses ranging from 1.5 to 15nm was reported in 1967.[19] The authors investigated the ferromagnetic resonance linewidth from 300K down to 4.2K observing a maximum value around 80K, whose amplitude enhanced with a surface oxidation process in the top interface of Py. The anomalies in the FMR-linewidth were explained in terms of valence exchange and exchange anisotropy mechanisms influences by surface oxidation. Diaz de Sihues *et al*.[20] studied the temperature dependence of the ferromagnetic linewidth as well as FMR frequency in polycrystalline $Ni_{50}Fe_{50}$ films grown on SiO_2 substrates with film thicknesses from 6 to 15nm. Both, the FMR frequency and linewidth exhibited a maximum around 100K. These experimental observations were explained in terms of a thermally induced spin reorientation transition at the Py interface due to variations of the surface anisotropy with temperature. Recently,[22] a similar variation in 25 nm single-layer Py films and unusually strong temperature dependences when Py was inserted into MTJs at low temperatures has observed. These observations were also interpreted within the frame of a thermally induced spin reorientation transition of the interface´s magnetic moments. These initial investigations create a number of questions that has to be clarified, particularly how temperature dependent dynamic and static properties of Py change when this films forms part of different multilayer stacks such as epitaxial MTJs, when it is grown with some preferential crystallographic orientation or when Py is grown over epitaxial layers. Our new experimental findings resolve some of the above points but also raises a few questions which will be addressed in forthcoming publications.

Let us first focus on the static and dynamics properties of the samples when Py is deposited on amorphous substrates and is inserted into a tunnel junction structure (A-MTJ1 and A-MTJ2). These MTJs show qualitatively similar temperature dependences in both static (peak followed by dip in saturation magnetization M_S*(T) with increasing temperature close to 60K) and in their dynamic ("knee"-like change of FMR resonance frequency measured at fixed field for temperatures around 60K) properties (see Figs. 6 and 10(a)). However, the effect is quantitatively less pronounced in the A-MTJ2. As we have mentioned above, the HRTEM images reveal that A-MTJ2 sample has substantially greater (111) textured than A-MTJ1, which is an indication on the inverse correlation between the degree of the Py texture and the magnitude of the low temperature anomalies in these MTJs. Indeed, a highly textured Py layer should posses an additional magnetocrystalline anisotropy partially suppressing the thermally induced reorientation transition.

On the other hand, static and dynamic properties of free Py layers are quantitatively and qualitatively different in comparison to those observed when Py is inserted into the tunnel junction (compare result in A-SL and in A-MTJ2, Figures 7 and 9). These differences have been explained before by considering possible influence of the dipolar coupling between the free and the pinned layer on the spins at the interfacing barrier layers when temperature is changed trough T-SRT.[22] The TEM images show indeed the presence of anticorrelated roughness regions along the Al_2O_3 barrier which may induce an antiferromagnetic coupling between the free and the pinned layer.[36] Within this scenario the main low temperature experimental features are understood as a consequence of competition between dipolar coupling and the thermally induced reorientation transition. While for $T<T_R$ the magnetic moments are out-of plane in both the free and pinned layer interfaces, these are in-plane for $T>T_R$. However, at $T\sim T_R$ it is possible to have non-equilibrium magnetic configuration in the anticorrelated regions that explain the knee-like enhancement in dynamics and the peak and the dip anomaly in static magnetic response (for more details in this model see ref. 22).

Thermally induced spin reorientation transition is quantitatively and qualitatively different for A-SL, E-SL and E-MTJ in comparison to A-MTJs. All these samples show similar temperature dependences in both static (peak anomaly) and dynamic properties (f_0 increases with decreasing temperature and small deviations of the linewidth respect to its constant value). From the X-Ray analysis we observe that Py is (111) textured in the A-SL and polycrystalline for the epitaxial substrates. In order to understand our experimental results, we suggest that crystallinity of Py layers depends on their proximity to the fully epitaxial MgO layer. This is, indeed, confirmed by the TEM images, where one observes a Py highly (111) textured very close to the MgO layer. In our view, the thermally spin reorientation transition in these Py films is still present at $T=T_R$, producing the peak anomaly in the static magnetic properties. For $T>T_R$ all the magnetic moments in the interface are in-plane while the surface spins push out-of-plane at $T<T_R$. However, the spin reorientation transition here is weak due to the crystalline character of Py at the interface with MgO which also induces magnetocristalline anisotropy. This is in good correspondence with our previous data for polycrystalline Py interfaces

(Py/SiO_2), where the thermally induced spin reorientation transition is *qualitatively* similar but much more pronounced in both the static and the dynamic properties[22] in comparison with new experimental results in the textured Py interfaces (Py/MgO). Finally, we note that peak in static magnetic properties is slightly shifted to higher temperatures in the epitaxial tunnel junction. Here, the dipolar coupling is much weaker in comparison with amorphous junctions due to the thicker barrier (5nm for epitaxial barrier compared with 1.8nm for the amorphous one). Some weak Néel coupling could however, influence the T-SRT in MTJs with MgO barrier changing value of T_R or influencing the non-equilibrium magnetic configuration at interface near $T=T_R$.

The micromagnetic simulations have been performed in Py thin films with surface anisotropy. Strong surface anisotropy was shown to be responsible for the "exchange-spring" effect, leading to slow dependence of the coercive field on temperature at low temperatures. The reorientation transition produces a strong disorder on the surface, associated with the maximum of the coercive field. This maximum could be potentially traced as some anomaly in the coercive field behavior of A-MTJs, however, hidden by the Py properties distribution, such as grain size, anisotropy, defects and magnetic interactions. A similar effect (competition between different energy contributions leading to an additional disorder) should be responsible for the maximum of the FMR linewidth.

In Conclusion, static and dynamic properties of thin Py films grown on insulating substrates or as a part of magnetic tunnel junctions reveal changes at low temperatures which could be attributed to a thermally induced spin reorientation transition. It is observed that the magnitude of this transition in both the magnetization dynamics and in the static magnetization notably depends on the microstructure of Py, which is influenced by the crystalline texture of the layers on which films are grown, The bulk of our main results suggest these effects could be a general characteristic for very different structures which incorporate Py films, even those with Py grown on superconducting substrates [compare data for samples A and B in Fig.4, of Ref. 37)]. Further detailed studies including detailed nanoscale analysis, such as neutron spectroscopy, however, are needed to reveal details of changes which occur in Py at low temperatures.

We thank M. J. Thornton for a critical reading of the manuscript. We acknowledge fruitful discussions with A.P. Levanyuk, V. Metlushko and F. García-Sánchez. This work was supported by the Spanish MEC MAT-2009-10139, MAT-2008-06517-C02-01, CSD-2009-00013, MAT2007-66719-C03-01, Consolider (CSD2007-00010 and CS2008-023) and Comunidad de Madrid (P2009/MAT-1726) contracts.

REFERENCES

[1] C. Chappert, A. Fert, and F. N. Van Dau, Nature Mater. **6**, 813 (2007).

[2] R. Guerrero, F. G. Aliev, Y. Tserkovnyak, T. Santos, and J. S. Moodera, Phys. Rev. Lett. **97**, 266601 (2006).

[3] F. G. Aliev, J. F. Sierra, A. A. Awad, G. N. Kakazei, D.-S. Han, S-K. Kim, V. Metlushko, B. Ilic and K. Y. Guslienko Phys. Rev. B, **79**, 174433 (2009).

[4] R. Guerrero, F. G. Aliev, R.Villar, J. Hauch, M. Fraune, G. Güntherodt, K. Rott, H. Brückl, and G. Reiss, Appl. Phys. Lett., 87, 042501(2005).

[5] M. Farle, Rep. Prog. Phys. **61**, 755 (1998).

[6] P. F. Carcia, J. Appl. Phys. **63**, 5066 (1988).

[7] D. Houssameddine, U. Ebels, B. Delaët, B. Rodmacq, I. Firastrau, F. Ponthenier, M. Brunet, C. Thirion, J.-P. Michel, L. Prejbeanu-Buda, M.-C. Cyrille, O. Redon and B. Dieny, Nat. Mat **6**, 447 (2007).

[8] *Ultrathin Magnetic Structures I*, edited by J. A. C. Bland and B. Heinrich, Springer, Berlin (1994).

[9] P. J. Jensen and K. H. Bennemann, Phys. Rev. B. **42**, 849 (1990).

[10] D. P. Pappas, K.-P. Kämper and H. Hopster, Phys. Rev. Lett. **64**, 3179 (1990). A. Enders, D. Peterka, D. Repetto, N. Lin, A. Dmitriev and K. Kern, Phys. Rev. Lett. **90**, 217203 (2003).

[11] M. Farle, W. Platow, A. N. Anisimov, P. Poulopoulos and K. Baberschke, Phys. Rev. B **56**, 5100 (1997).

[12] G. André, A. Aspelmeier, B. Schulz, M. Farle and K. Baberschke, Surface Science, **326**, 275 (1995).

[13] S.A. Gusev, A.A. Fraerman, D.B. Rozenstein and M.G. Teitelman, Physics Letters A, **198**, 437 (1995).

[14] P. E. Tannenwald and M. H. Seavey, Jr. Phys. Rev. **105**, 377 (1957).

[15] T. J. Silva, C. S. Lee T. M. Crawford and C. T. Rogers, J. Appl. Phys. **85**, 7849 (1999).

[16] S. Y. An, P. Krivosik, M. A. Kraemer, H. M. Olson, A. V. Nazarov and C. E. Patton, J. Appl. Phys. **96**, 1572 (2004).

[17] D. J. Twisselmann and R. D. McMichael, J. Appl. Phys. **93**, 6903 (2003).

[18] S. S. Kalarickal, P. Krivosik, M. Wu, C. E. Patton, M. L. Schneider, P. Kabos, T. J. Silva and J. P. Nibarger, J. Appl. Phys. **99**, 093909 (2006).

[19] C. E. Patton and C. E. Wilts, J. Appl. Phys. **38**, 3537 (1967).

[20] M. Díaz de Sihues, P. J. Silva and J. R. Fermin, Physica B, **354**, 361 (2004).

[21] P. Lubitz, M. Rubinstein, J. J. Krebs, and S.-F. Cheng, J. Appl. Phys. **89**, 6901 (2001).

[22] J. F. Sierra, V. V. Pryadun, F. G. Aliev, S. E. Russek, M. García-Hernández, E. Snoeck and V. V. Metlushko, Appl. Phys. Lett. **93**, 172510 (2008).

[23] J.F Sierra, F.G. Aliev, R. Heindl, S. E. Russek and W. H. Rippard, Appl. Phys. Lett. **94**, 012506 (2009).

[24] M. Shaw, R. Geiss and S. E. Russek, Appl. Phys. Lett. **89**, 212503 (2006).

[25] G. X. Miao, J. Y. Chang, M. J. van Veenhuizen, K. Thiel, M. Seibt, G. Eilers, M. Münzenberg and J. S. Moodera, Appl. Phys. Lett. **93,** 142511 (2008).

[26] P. Vavassori, E. Angeli, D. Bisero, F. Spizzo and F. Ronconi, Appl. Phys. Lett. **79**, 2225 (2001).

[27]K.-Y Wang, M. Sawicki, K. W. Edmonds, R. P. Campion, S. Maat, C. T. Foxon, B. L. Galangher and D. Dietl, Phys. Rev. Lett. **95**, 217204 (2005).

[28] G. Garreau, E. Beaurepaire, K. Ounadjeda and M. Farle, Phys. Rev. B, **53**, 1083 (1996).

[29]Y. Yafet and E. M. Georgy, Phys. Rev. B **38**, 9145 (1988).

[30]C. Won, Y. Z. Wu, J. Choi, W. Kim, A. Scoll, A. Doran, T. Owens, J. Wu, X. F. Jin, H.W. Zhao and Z. Q. Qui, Phys. Rev. B. **71**, 224429 (2005).

[31]M. Carubelli, O. V. Billoni, S. Pighin, S. A. Cannas, D. Stariolo and F. A. Tamarit, Phys. Rev. B **77**, 134417 (2008).

[32] F. García-Sánchez, PhD thesis (Universidad Autónoma de Madrid, 2007) http://www.icmm.csic.es/magsim

[33] M. R.Gibbons, J. Magn. Magn. Mat. **186**, 389 (1998).

[34] H. B. Callen and E. Callen, J. Phys. Chem. Solids. **27**, 1271 (1966).

[35] P. Asselin, R. F. L. Evans, J. Barker, R. W. Chantrell, R. Yanes, O. Chubykalo-Fesenko, D. Hinzke, U. Nowak, Phys. Rev. B. **82**, 054415 (2010).

[36] P. Vargas, D. Altbir, Phys. Rev. B. **62**, 6337 (2000).

[37] C. Bell, S. Milikisyants, M. Huber, J. Aarts, Phys. Rev. Lett. **100**, 047002 (2008).

FIGURE CAPTIONS

FIGURE 1. Cross section TEM images for amorphous samples. (a) Amorphous single-layer (A-SL): Al_2O_3(1.8)/ $Co_{60}Fe_{20}B_{20}$(2)/$Ni_{80}Fe_{20}$(23)/Ta(5)/Ru(5) and (b) Amorphous magnetic tunnel junction 2 (A-MTJ2): Ta(5)/Cu(5)/Ta(5)/Ru(2)/$Ir_{20}Mn_{80}$(10)/$Co_{90}Fe_{10}$(3)/Al_2O_3(1.8)/$Co_{60}Fe_{20}B_{20}$(2)/$Ni_{80}Fe_{20}$ (23)/Ta(5)/Ru(5). The dashed lines indicate the barrier profile. Anticorrelated roughness in the barrier is marked with arrows.

FIGURE 2. Cross section TEM images for epitaxial samples: (a) Epitaxial single layer (E-SL): MgO(10)/$Ni_{80}Fe_{20}$(30)/Al_2O_3(5). (b) Epitaxial magnetic tunnel junction (E-MTJ): MgO(10)/Fe(20)/MgO(5)/$Ni_{80}Fe_{20}$(30)/Al_2O_3(5). The dashed lines indicate the barrier profile. A zoom image of the Fe/MgO interface and the epitaxial structure of the MgO is shown in the left-bottom part of the image.

FIGURE 3. X-ray diffraction patterns for samples A-MTJ1, A-MTJ2 (top panel) and A-SL (bottom panel).

FIGURE 4. X-ray diffraction patterns for samples E-MTJ (top panel) and E-SL (bottom panel).

FIGURE 5. (a) Imaginary part of the FMR signal (see Ref.18) for two different temperatures measured in an applied field of 20mT for A-MTJ1 and (b) A-MTJ2. Resonance frequency vs. magnetic field at 300K (open symbols) and 5K (full symbols) for A-MTJ1(c) and for A-MTJ2 (d). The inset in (c) shows the scheme of the MTJs, indicating the value of f_0 measured corresponds to the uniform mode of the free layer magnetization.

FIGURE 6. Contour plots of the FMR peak (f_0) as a function of temperature and applied field for amorphous A-MTJ1 (a) and A-MTJ2 (b) samples. (c) Temperature dependent FMR peak for A-MTJ1 at three different applied fields (marked with white dashed lines in (a)). (d) Temperature dependent FMR peak for A-MTJ2 at two different applied fields. Shadow regions in (c) and (d) indicate the "knee-like" enhancement of f_0.

FIGURE 7. Contour plots of the FMR linewidth (Δf_0) at different temperatures and applied fields for A-MTJ1 (a) and A-MTJ2 (b). Temperature dependence of the Δf_0 at three different applied fields for A-MTJ1(c) and A-MTJ2 (d).

FIGURE 8. (a) FMR peak as a function of temperature for amorphous structures. (b) FMR peak as a function of temperature for epitaxial structures. Lines are "guides to the eye". Shadow area shows the region whit a change in slope.

(c) FMR linewidth as a function of temperature for amorphous structures. (d) FMR linewidth as a function of temperature for epitaxial structures. All data correspond to 20mT applied field.

FIGURE 9. (a) Magnetization vs. magnetic field for A-MTJ2 sample measured at three different temperatures near T_R. (P) denotes the parallel state and (AP) the antiparallel state of the sample. (b) Magnetization curves for A-SL sample near T_R. The inset shows the zoom image of the magnetization curve near the saturation region

FIGURE 10. Temperature dependence of M^*_S normalized by its value at 5K near the spin reorientation temperature for magnetic tunnel junctions (a) and single-layer films (b). The insert in (a) show the zoom images for the E-MTJ sample.

FIGURE 11. Coercive field vs. temperature for A-MTJ1 and A-SL samples. The inset shows the derivative curve of H_C for A-MTJ1. The arrow indicates the weak anomaly in the coercive field.

FIGURE 12. Modelling results of the coercive field as a function of temperature in a Py thin film with surface anisotropy.

FIGURE 13. Part of the magnetic moment configurations corresponding to the simulated remanence of Py magnetic thin films with surface anisotropy in the model A (a) T= 300 K (ZX plane view) (b) T=450 K (ZY plane view, spin reorientation transition).

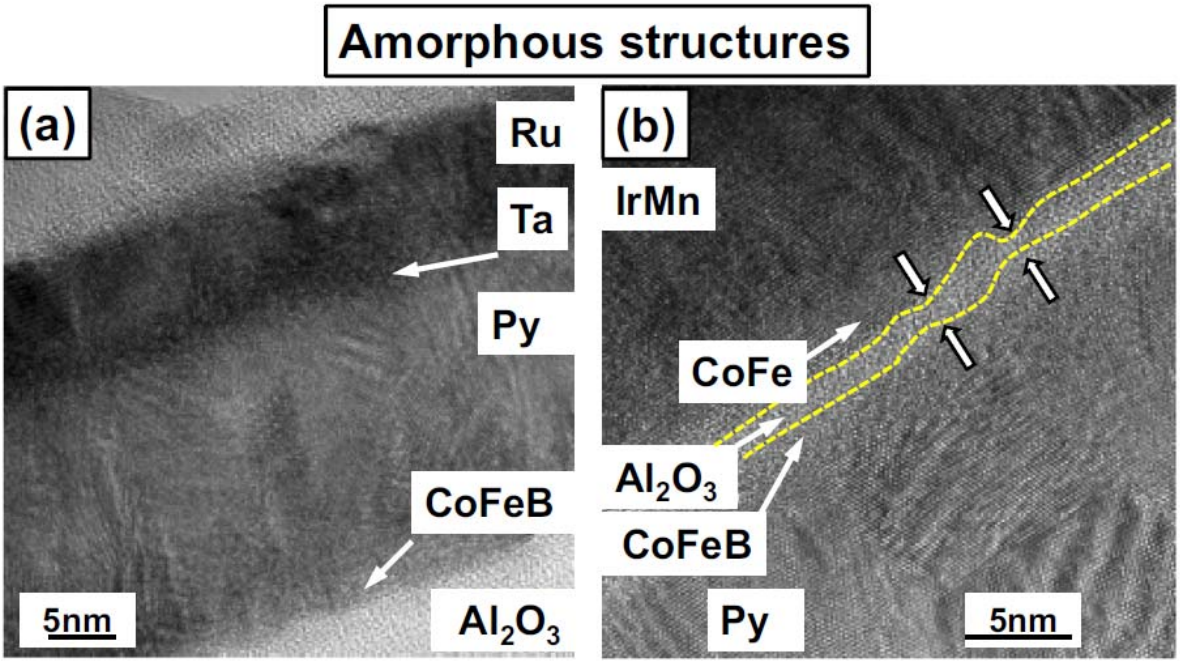

Figure 1 Sierra et al.

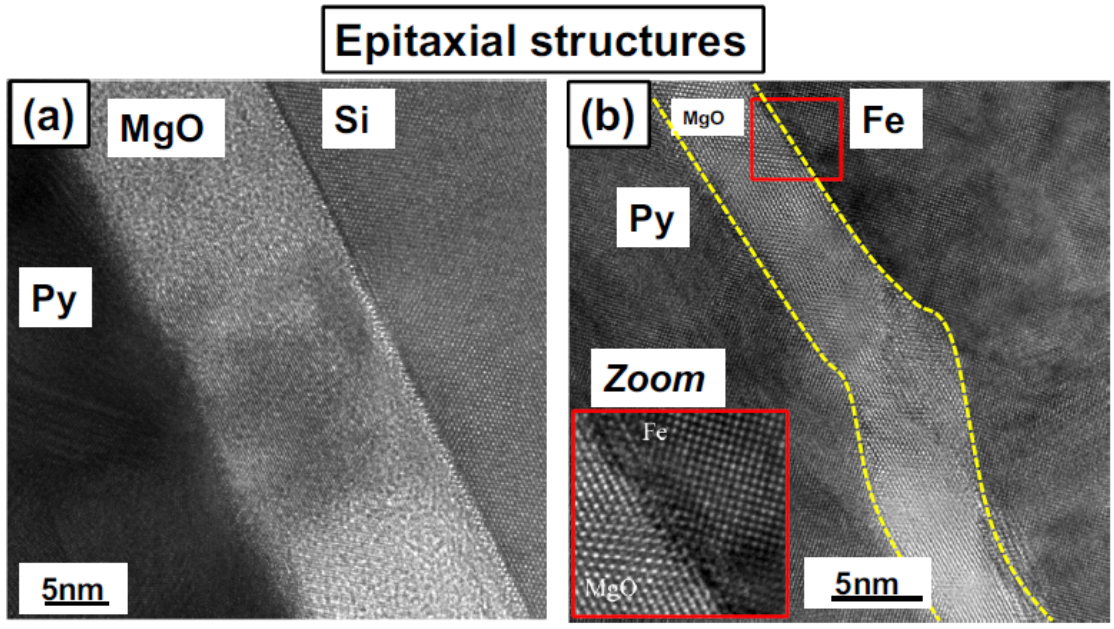

Figure 2. Sierra et al.

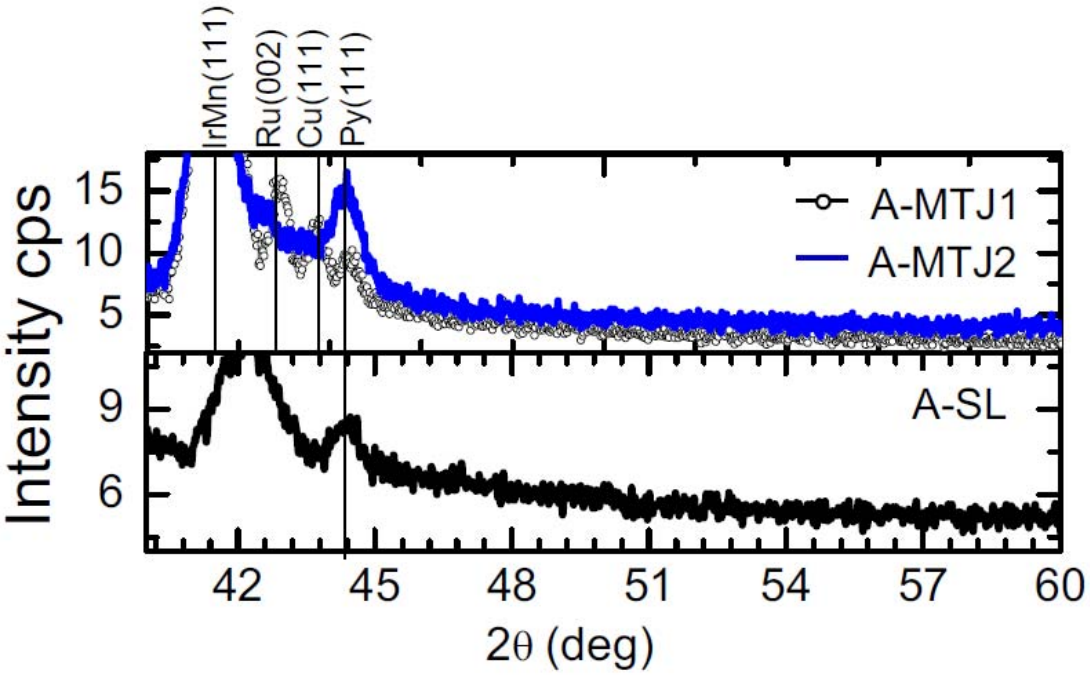

Figure 3. Sierra et al.

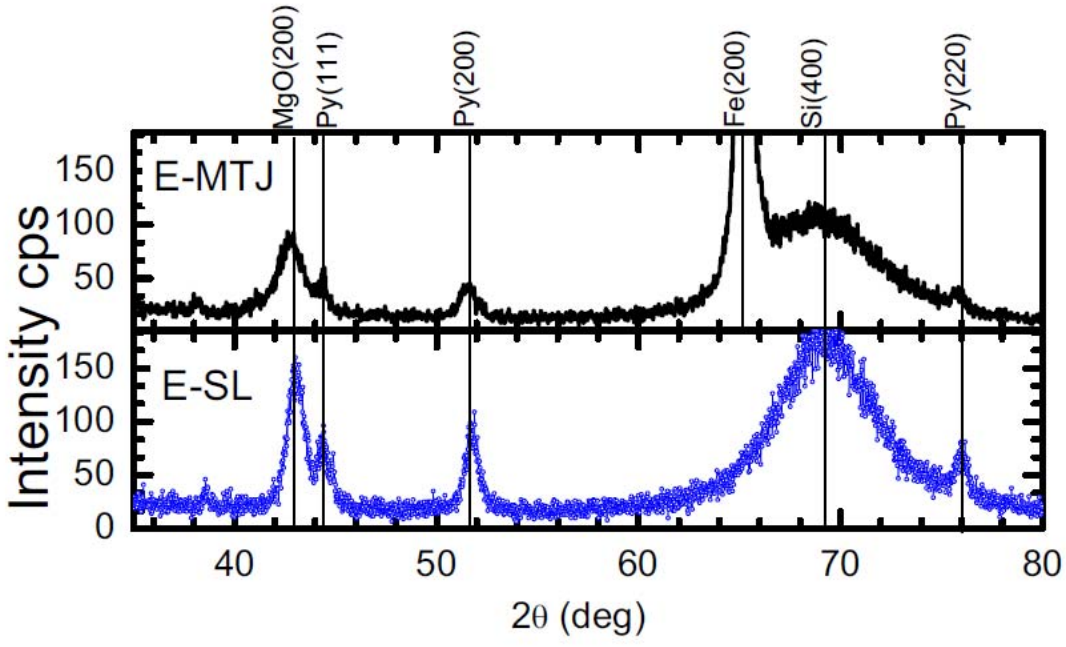

Figure 4. Sierra et al.

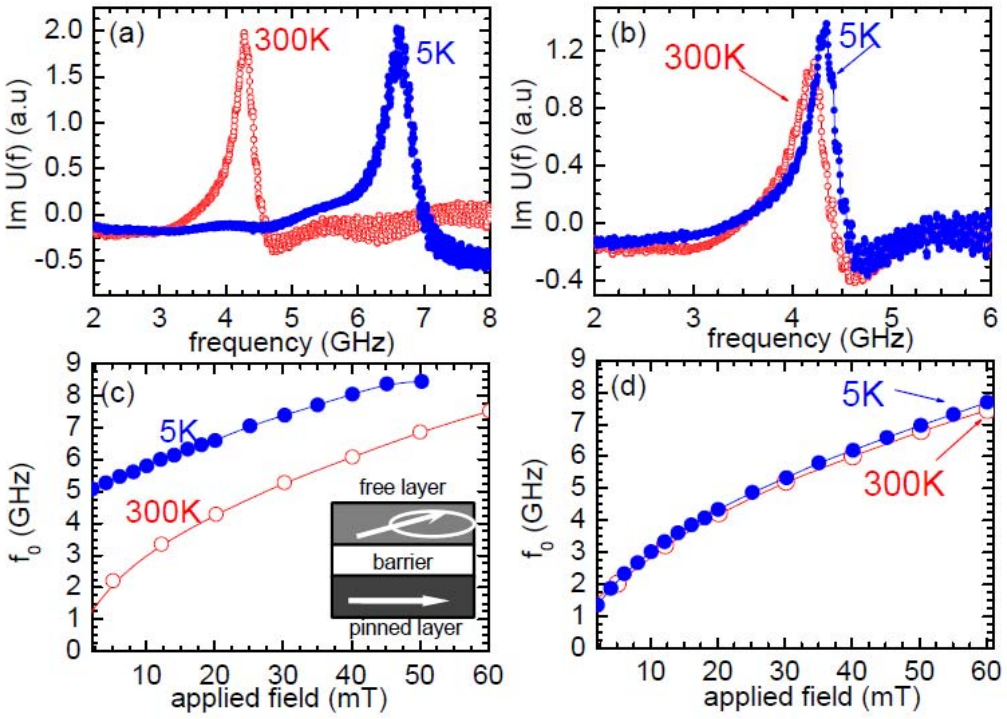

Figure 5. Sierra et al.

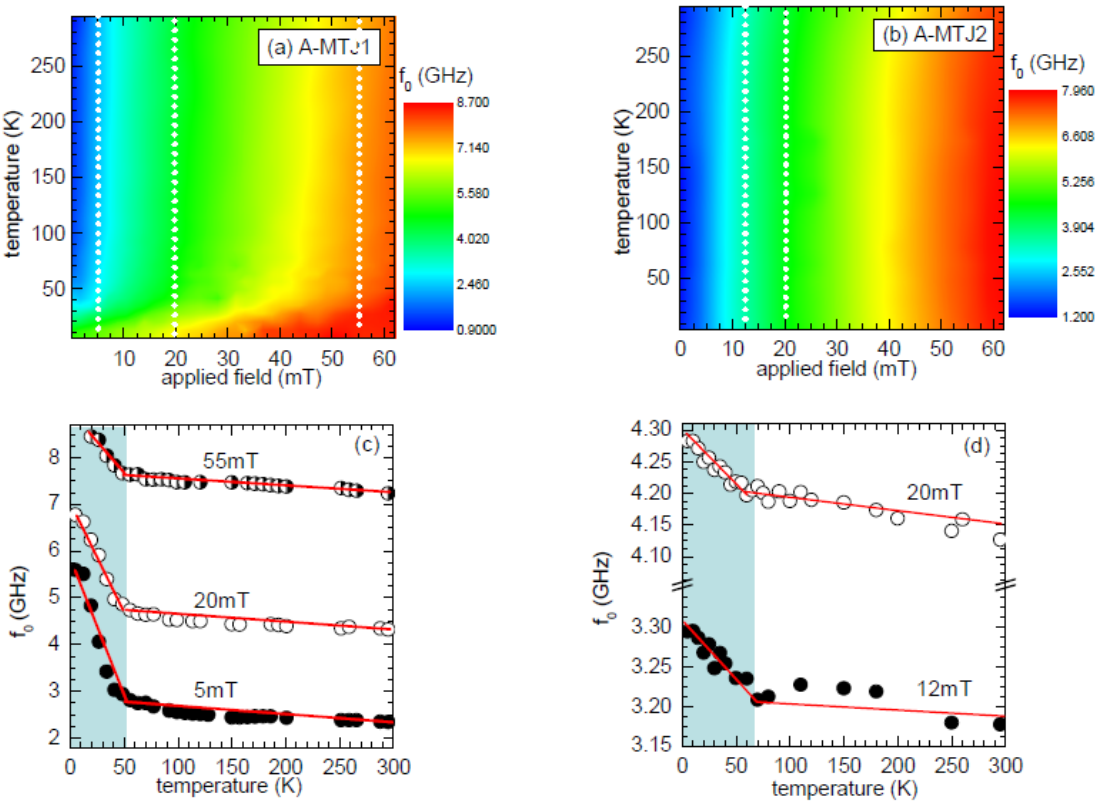

Figure 6. Sierra et al.

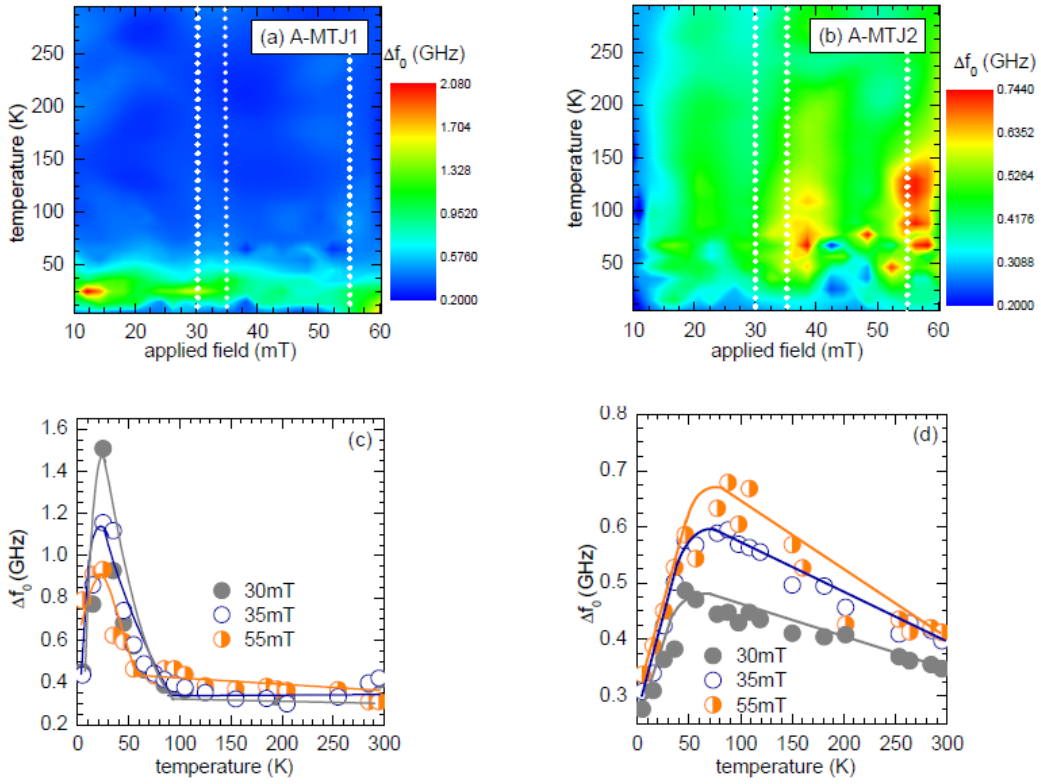

Figure 7. Sierra et al.

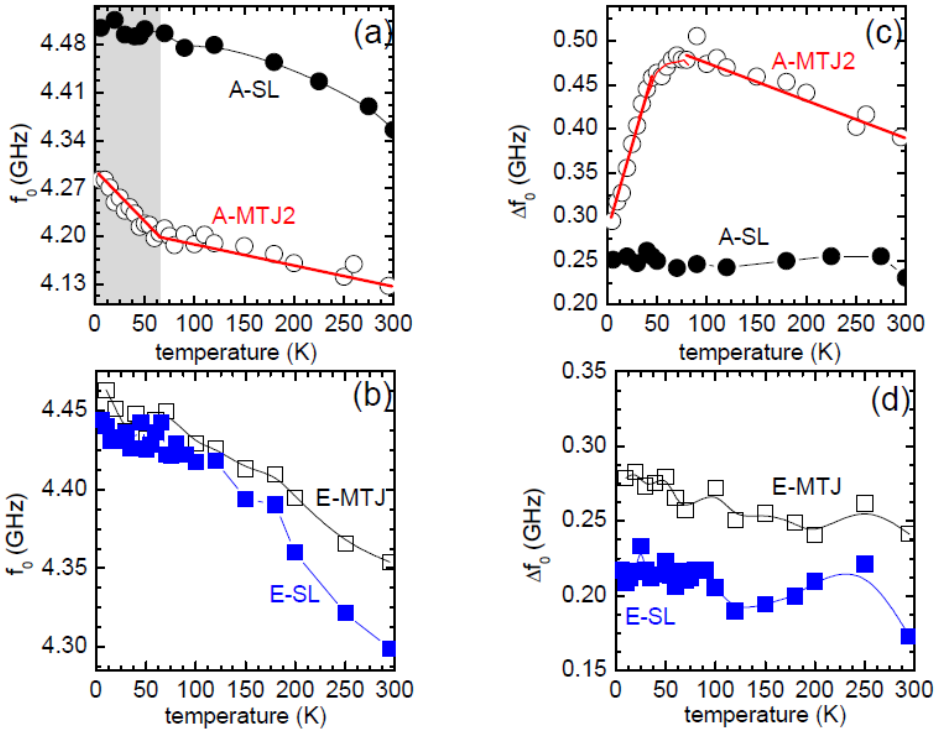

Figure 8. Sierra et al

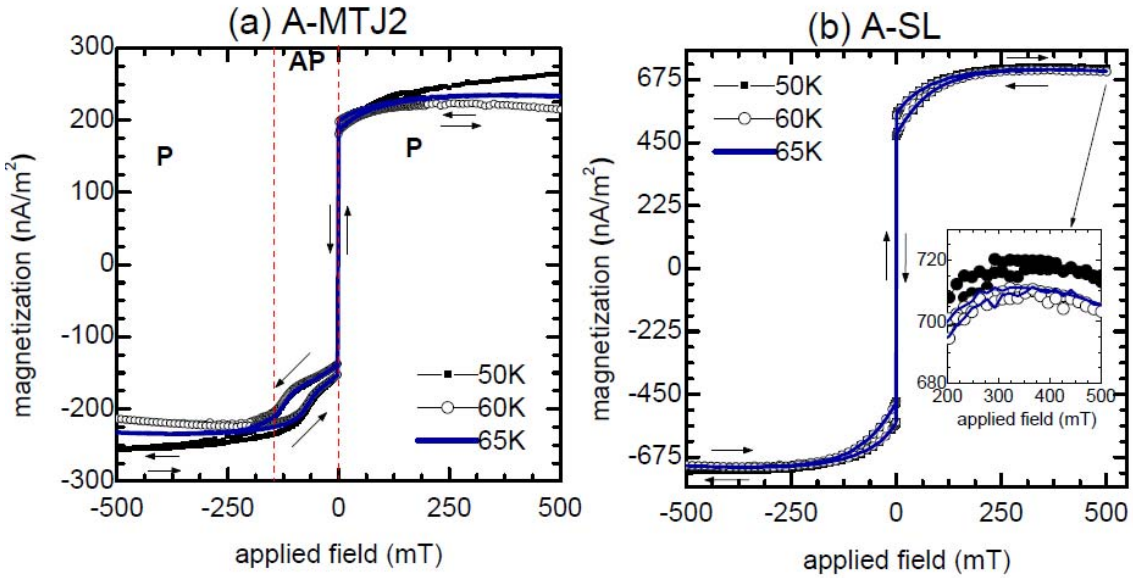

Figure 9. Sierra et al.

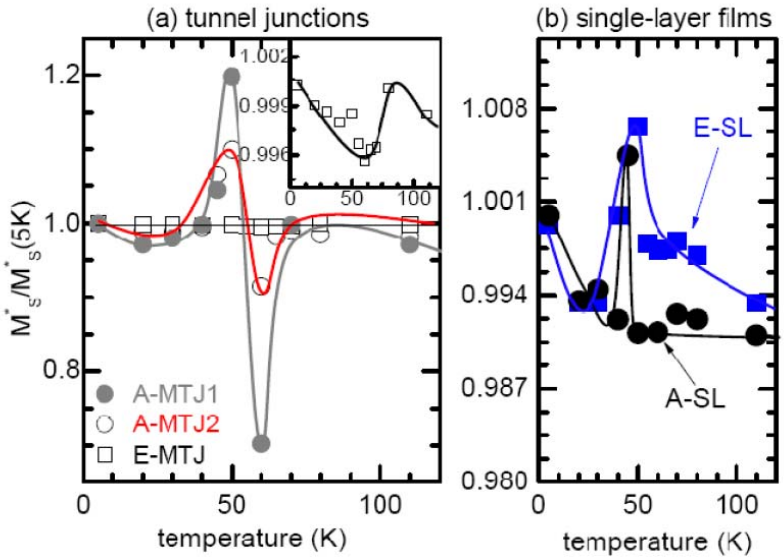

Figure 10. Sierra et al

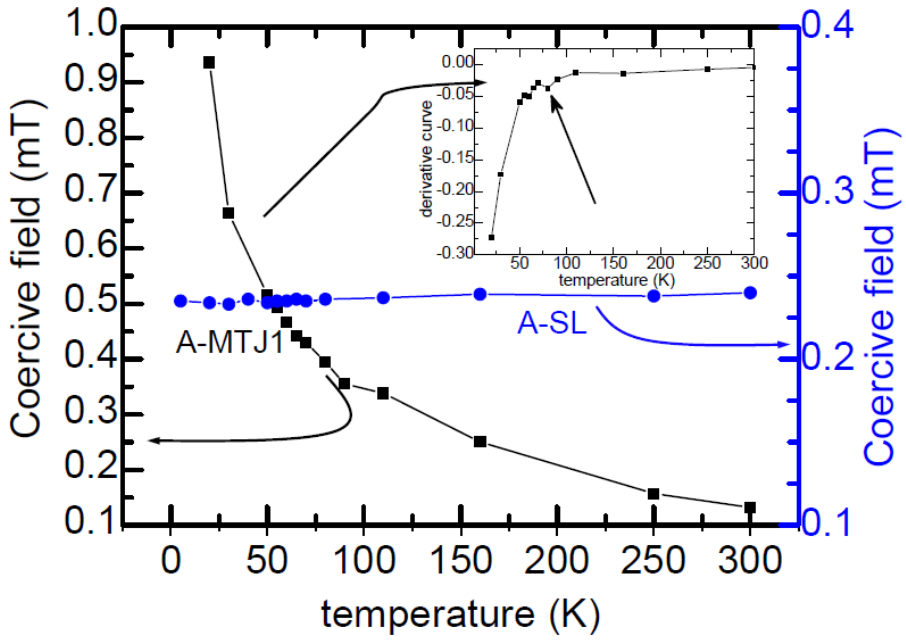

Figure 11. Sierra et al.

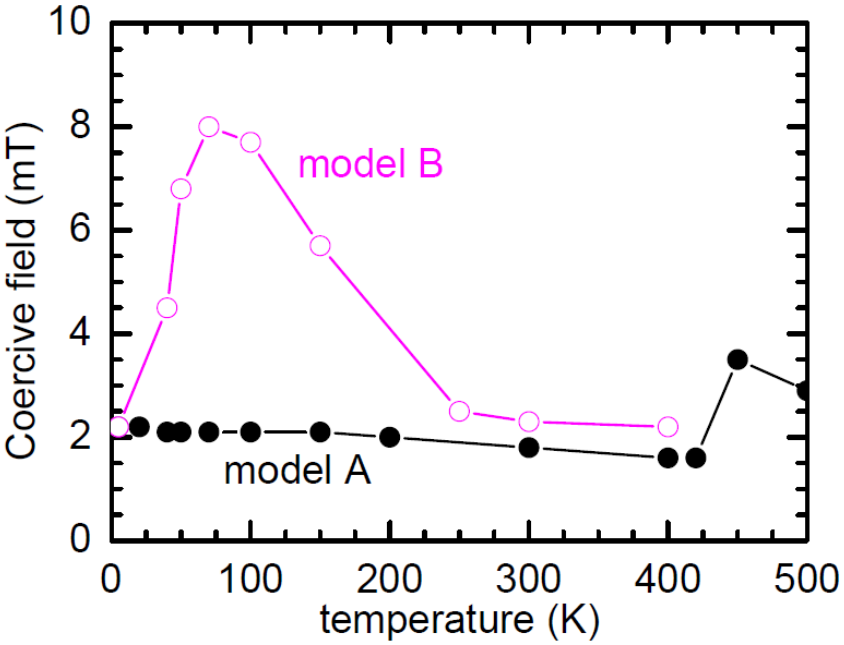

Figure 12. Sierra et al.

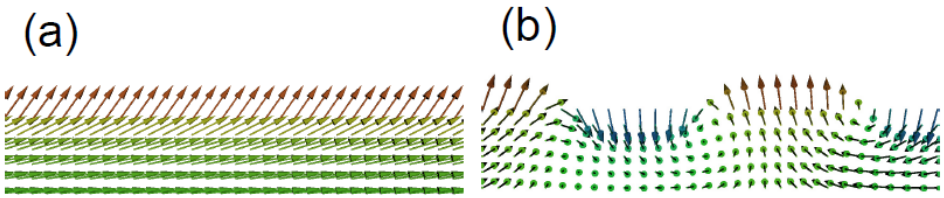

Figure 13. Sierra et al.